



D5.1: Dynamic active constraint construction

SMARTsurg

SMart weArable Robotic Teleoperated surgery

D5.1: Dynamic active constraint construction

Due date (First Release): M18

Abstract:

The present document is a deliverable of the SMARTsurg project, funded by the European Commission's Directorate-General for Research and Innovation (DG RTD), under its Horizon 2020 Research and innovation programme (H2020). This deliverable aims at presenting the results of Task T5.1 until M18 of the project. It is developed within the scope of WP5.

D5.1 describes the processes for the construction of the active constraints (i.e. safety area) corresponding to the anatomical-functional regions that must not be damaged during the Robot-Assisted surgery, due to unwanted contact with the surgical tool.

In order to design the constraints, the user can either choose pre-operative models derived from medical image segmentation or design them intra-operatively, using the master arm (or other input devices) to virtually contour the safety areas of interest on the stereo-images. First attempt to software development have been done and the preliminary results are reported. As the task 5.1 progresses toward month 26, the software will be upgraded.

As first demonstration scenario, partial nephrectomy was chosen. Phantom dataset and physical phantom construction was made to test the active constraints construction methods developed.

This release represents the preliminary achievements at month 18 and will be updated along the task 5.1 until month 26 (as per implementation description)



Reference : SMARTsurg-WP1-D1.1-v0.1-UWE
Version : 1.0
Date : 2018.06.01
Page : 2

D5.1: Dynamic active constraint construction

Dissemination Level		
PU	Public	x
PP	Restricted to other programme participants (including the Commission Services)	
RE	Restricted to a group specified by the consortium (including the Commission Services)	
CO	Confidential, only for members of the consortium (including the Commission Services)	



D5.1: Dynamic active constraint construction

Document Status











Document Title	Dynamic active constraint construction
Version	0.3
Work Package	5
Deliverable #	5.1
Prepared by	POLIMI
Contributors	POLIMI
Checked by	CERTH
Approved by	UWE
Date	02/07/2018
Confidentiality	PU



Reference : SMARTsurg-WP1-D1.1-v0.1-UWE
Version : 1.0
Date : 2018.06.01
Page : 4

D5.1: Dynamic active constraint construction

Contact Points

Coordinator		
 University of the West of England	University of the West of England/ Bristol Robotics Laboratory T Building, Frenchay Campus BS16 1QY Bristol, UK	Tel: +44 117 32 81301 E-mail: Sanja.Dogramadzi@brl.ac.uk Website: www.brl.ac.uk/research/researchthemes/medicalrobotics.aspx
Partners		
 Information Technologies Institute	Centre for Research and Technology Hellas / Information Technologies Institute Building A - Office 1.1A 6th km Charilaou - Themi, 57001 Thessaloniki, Greece	Tel.: +30 2311 257777 Fax: +30 2310 474128 E-mail: tzovaras@iti.gr Website: www.iti.gr
 POLITECNICO MILANO 1863	Politecnico di Milano Department of Electronics, Information and Bioengineering Building 32.2 Via G.Ponzio 34/5 Milan, Italy	Tel.: +39 022 399 3371 E-mail: giancarlo.ferrigno@polimi.it Website: www.nearlab.polimi.it
 Bristol Urological Institute	North Bristol National Health Service Trust/ Bristol Urological Institute Brunel Building, Southmead Hospital BS10 5NB Bristol, UK	Tel.: +44 117 4140898 E-mail: anthony.koupparis@nbt.nhs.uk Website: www.nbt.nhs.uk/bristol-urological-institute
 University of BRISTOL	University of Bristol Translational Biomedical Research Centre Senate House, Tyndall Avenue BS8 1TH Bristol, UK	Tel.: +44 117 3423286 E-mail: r.ascione@bristol.ac.uk Website: www.bristol.ac.uk/health-sciences/research/tbrc
 IEO Istituto Europeo di Oncologia	European Institute of Oncology Division of Urology Via Ripamonti, 435 20141 Milan, Italy	Tel.: +39 0257489516 E-mail: ottavio.decobelli@ieo.it Website: www.ieo.it
 TheMIS THESSALONIKI MINIMALLY INVASIVE SURGERY ORTHOPAEDIC CENTER	TheMIS Orthopaedic Center 6 Adrianoupoleos St. 55133 Thessaloniki, Greece	Tel.: +30 2310 223 113 E-mail: papacostas@the-mis.gr Website: www.the-mis.gr
 cybernetix A TechnipFMC Company	Cybernetix 306 Rue Albert Einstein 13882 Marseille, France	Tel.: +33 491 210 484 E-mail: jvandenbosch@cybernetix.fr Website: www.cybernetix.fr
 Optinvent	Optinvent R&D Department Avenue des Buttes de Coesmes 80 35700 - Rennes, France	Tel.: +33 299871066 E-mail: khaled.sarayeddine@optinvent.com Website: www.optinvent.com
 HIT HYPERTECH INNOVATIONS	HIT Hypertech Innovations Agiou Nikolaou 33 2408, Nicosia, Cyprus	Tel./Fax: +357 22251217 E-mail: contact@hit-innovations.com Website: www.hit-innovations.com



D5.1: Dynamic active constraint construction

Document Change Log

Each change or set of changes made to this document will result in an increment to the version number of the document. This change log records the process and identifies for each version number of the document the modification(s), which caused the version number to be incremented.

Change Log	Version	Date
First draft	0.1	June 15, 2018
Updated	0.2	June 27, 2018
Updated with partner's feedback	0.3	June 30, 2018
Submitted	1.0	July 2, 2018



D5.1: Dynamic active constraint construction

Table of Contents

1	Introduction.....	10
1.1	Objective and Scope	10
1.2	Document Structure.....	14
1.3	Reference Documents	14
1.4	Acronyms and Abbreviations	15
2	Registration	16
2.1	Pair-point registration (Rigid Landmark-based registration)	16
2.2	Surface-based rigid registration.....	16
2.3	Deformable surface registration	17
3	Intra-operative Graphical User Interface (GUI)	20
3.1	GUI Main window	21
3.2	Preoperative Models Window	22
3.3	AC window	22
3.4	Vital Signals Window	23
3.5	Camera Window.....	23
3.6	Repository with code	24
4	AC definition.....	25
4.1	Pre-operative AC definition	25
4.2	Intra-operative AC definition.....	27
5	Datasets.....	33
6	Conclusion.....	34
7	References	35



D5.1: Dynamic active constraint construction

List of Figures

Figure 1 Example (a) regional and (b) guidance constraints. Obstacles are shown in grey and the constraints in black (striped area on the left). Picture from (Bowyer, Davies, & Rodriguez y Baena, 2014)	10
Figure 2 f_k attempts to guide the tool tip at x_k towards the closest point on the reference path.	11
Figure 3 AC can be defined either on pre-op models or on intra-operative models. Both are registered using a rigid or deformable approach. AC provide repulsive force fields (AC enforcement – T5.2).	13
Figure 4 Pair-point registration of the kidney model to the intra-operative kidney point cloud. (Left) The pre-operative point cloud (M) is shown in blue and the simulated intra-operative point cloud (F) in pink. Anatomical landmarks, manually selected through a graphic-user interface, are shown in green both for M (L_M) and for F (L_F). (Right) The computed pair-point registration is applied to register the pre-operative point cloud into the intra-operative scene.	16
Figure 5 The VF (upper panel) describes surface-based deformable registration. VF can be seen as a grid superimposed to the pre-operative point set, in which each block has associated a displacement vector, representing the direction and the size of the translation applied to what is inside that block. In the lower panels, the deformed (right) and initial (left) position of exemplary points is reported.	17
Figure 6 FFD results. (Upper panel on the left) Initial situation: the blue point cloud refers to the pre-operative model and the pink point cloud to the intra-operative phantom-kidney surfaces. (Upper panel in the middle) Rigid registration with ICP, the initial alignment was performed with the pair-point registration. (Upper panel on the right) Registration refinement was performed with surface-based deformable registration. On the lower panel, a slice is represented for better visualization: (a) Pre-operative model vertexes (blue) and intra-operative point cloud (red). The registration is obtained with (b) iterative closest points (ICP) and (c) free-form deformation based on B-splines.	18
Figure 7 RMSE percentage variation after applying ICP and FFD algorithms. A better performance of FFD is evident from the Box plots.	19
Figure 8 Block scheme of the GUI. Orange blocks represent the hardware components, green blocks represent high-level components, yellow blocks represent middleware and blue blocks represent the programming languages used for the implementation. Solid arrows are used to show how blocks communicates each other, while dashed lines to show how a human interact with the system.	20
Figure 9 Full-preoperative-models window (with VR environment rendering) for models manipulation and exploration. The top image shows the positioning of the window during the surgery. The bottom line represent three different modalities of visualization: mesh with low transparency, wireframe and point-cloud.	22
Figure 10. On the upper right corner the AC windows is shown. AC can be visualized and hidden using the “Visual AC” toggle. The “Actual AC” toggle is used to switch on/off force rendering of the active constraints. A yellow line is reported, which delimits a safety area on a plane placed between observer and 3D scene (see also Figure 17 in 4.2)	23
Figure 11 vital signs window with ECG signal	23
Figure 12 GUI for model segmentation (3D Slicer)	25



D5.1: Dynamic active constraint construction

Figure 13 Generated 3D model from the segmented organs (bone, liver, spleen, kidneys).....	26
Figure 14 Pre-operative organ models for constraint definition. Straw yellow: stomach; orange: liver; green: left kidney (with the cancer highlighted in brown); blue: inferior vena cava and renal veins; red: aorta; pink: ureters; intense yellow: bladder; white: chest and pelvis bones.	26
Figure 15. AC design in virtual world where the surfaces are represented with polygonal meshes. The pointer for actual surface brushing is indicated with a small white sphere. Picture refers to a kidney surface (reddish background) on which an esophytic tumour is located and the renal arteries enter the parenchyma.....	28
Figure 16 AC point cloud (light green spots) has been designed on the virtual surface on the renal arteries.	29
Figure 17. Structure of the projection of 3D scene on the plane where safety areas are drawn.	30
Figure 18. Projecting Point cloud on a 2D plane where the AC contour is then drawn (polygon bounding the green area) and projecting the points inscribed in green area back to the 3D scene, identifies the points belonging to the AC as a point cloud (green spots).	30
Figure 19. Point in polygon problem	31
Figure 20: (1) a virtual plane is defined between the observer (intersection of the grey lines) and the object (blue 3D-points); (2) 3D-points are projected on the virtual plane; (3) an area is drawn on the plane to define the AC; (4) points within the area are identified and (5) associated to their corresponding 3D-point to define the 3D-AC (6)	32
Figure 21 Experimental setup for dataset acquisitions at POLIMI.....	33



D5.1: Dynamic active constraint construction

Executive Summary

The present document is a deliverable of the SMARTsurg project, funded by the European Commission's Directorate-General for Research and Innovation (DG RTD), under its Horizon 2020 Research and innovation programme (H2020). This deliverable aims at presenting the results of Task T5.1 ("Dynamic active constraints construction") achieved at month 18. Since Task 5.1 will run up to month 26, new updated releases will be delivered.

As stated in the GA the main objective of T5.1 is the definition and intra-operative update of the active constraints, i.e. the regions that have to be avoided during the surgery, such as vessels and nerves. The definition and localization of such regions allow increasing the intervention safety. T5.1 is indeed an action required to achieve KPI-6, the target value of which is "a safe distance margin from any sensitive anatomical structures can be maintained".

In order to design the constraints, the user can either choose pre-operative models derived from medical image segmentation or design them intra-operatively, using the master arm (or other input devices) to virtually contour the safety areas of interest on the stereo-images. First attempt to software development have been done and the preliminary results are reported.

The main challenging scientific issues are related to:

- Intra-operative user-friendly definition of visible constraints and real-time position update
- Constraints displacement real-time prediction (for a suitable time) in case the constrained region is not perfectly visible to the stereo-cameras.

In order to reach the first goal, POLIMI implemented:

- Methods for anatomical regions segmentation, starting from pre-operative medical images of the organs of interest (similarly to D3.3).
- Methods for registering the pre-operative models to the intra-operative models (implemented in T3.1) using rigid and deformable registration.
- A Unity-based graphical user interface general framework for allowing the user to interact with the intra-operative models and define constrained regions on them (and other utility functions as the display of constructed constrains, biological signals representation, etc.).
- Phantom organs CAD (.stl) and object (.obj) files from medical images, for testing and organs volume representation in the interface. Molds have been designed for silicon organ production.

The suitability of the developed methods for use in the integrated system is still to be verified. The Task 5.1 requires that the actual methods undergo further research, testing and tuning to achieve the expected results. A more thorough presentation and description of the active constraint construction methods for the integrated system will be reported in the updated versions of the D5.1, from now to M26.



1 Introduction

1.1 Objective and Scope

In order to increase the safety of the robotic surgical procedure, constrained regions can be defined, known as Active Constraints (AC - or virtual fixtures).

AC are a control concept, whereby “abstract sensory information [is] overlaid on top of reflected sensory feedback from remote environments” (Rosenberg, 1993; Rosenberg, 1993): augmenting haptic feedback from the slave to the master in a teleoperation system, virtual fixtures can reduce mental workload, task time and errors, as stated in the review paper by (Bowyer et al., 2014). The same authors proposed the following AC classification:

- AC in Teleoperation/ hands-on controlled interface
- AC control in Admittance/ impedance
- Regional AC/ guidance AC (Figure 1)
- Attractive AC/ repulsive AC
- Unilateral AC/ bilateral AC
- Static AC/ dynamic AC. Dynamic AC have to be implemented when the geometry modifies as a result of environmental changes.

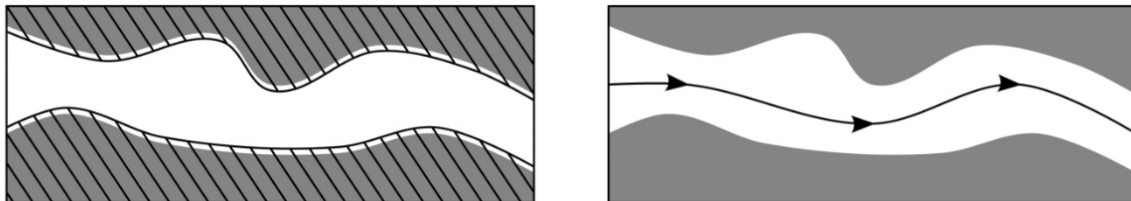


Figure 1 Example (a) regional and (b) guidance constraints. Obstacles are shown in grey and the constraints in black (striped area on the left). Picture from (Bowyer, Davies, & Rodriguez y Baena, 2014)

Guidance virtual fixtures were used to assist knot tying in robotic laparoscopy (Chen et al., 2016) and to help co-manipulated tasks. POLIMI had previous experiences in how to construct active constraints, which is the target of this deliverable, since they implemented viscosity-based dynamic guidance constraint that continuously redirected the tool's motion towards the reference path (Figure 2). (Enayati et al., 2016). Other examples of regional constraints in complementary field were designed in (Marinho et al., 2018) in order to increase the safety during deep brain neurosurgery and endonasal surgery.



D5.1: Dynamic active constraint construction

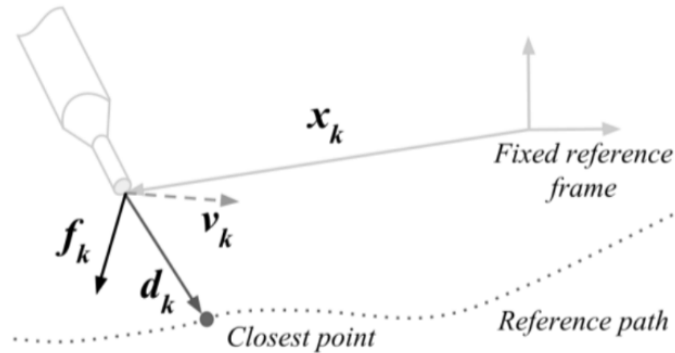


Figure 2 f_k attempts to guide the tool tip at x_k towards the closest point on the reference path.

In the framework of the SMARTsurg implementation, according to Deliverable D2.1 we foresee **regional dynamic constraints** in the following anatomical districts (Table 1):

Table 1 List of SMARTsurg scenarios and AC regions

	Scenario	Phase	Step	AC
1	Robot-assisted partial nephrectomy (RAPN)	5. Tumor excision	5.2 Expose the pedicles and clamp the renal artery	AC could be used to prevent injuries to the renal arteries.
2	Robot-assisted radical prostatectomy (RARP)	14. Lymph node dissection	14.1 Dissect the lymphatic tissue bluntly 14.2 Divide the main lymphatic trunks 14.3 Remove the lymph nodes	AC could be used to prevent injury to the common iliac vessels, internal and external iliac vessels, and genitofemoral nerve.
3	Robot-Assisted cystectomy and intracorporeal Reconstruction with ileal conduit or orthotopic neobladder (RARC)	2. Lymphadenectomy	2.1 Start dissection at the common iliac vessels where they are crossed by the ureter and proceed distally 2.2. Clear Lymphatic tissue from the ureter downwards	The AC could be used to prevent injury to major vessels
4	Robot-assisted Partial Lateral Meniscectomy (RaPLM)	4 Partial Meniscectomy	4.1 Insert the punch	Active constraints is implemented to prevent the injury to meniscus rim and to cut the minimum meniscus e.g. meniscus flaps could be labelled for the active constraints.



D5.1: Dynamic active constraint construction

5	Robot-assisted Repair of Partial Lateral Meniscus Tear (RaLMR)	4 Meniscal repair	4.1 Meniscal repair a. All inside technique OR b. Inside-out technique OR c. Outside-in technique	Active constraints could be used to do repair accurately in red zone, white zone and red-white zone.
6	Cardiac surgery	Left Internal Mammary Artery	1.3 Develop the incision in parallel to the LIMA 1.4 Cauterize sternal branches 1.5 Detach full LIMA pedicle	Active constraints could be useful for preventing the burning of LIMA while cauterising the sternal branches or when using the diathermy

The representative scenario chosen by POLIMI for the planned demonstrators is:

1 RAPN (Phase 5. Tumor excision, Step 5.2 Expose the pedicles and clamp the renal artery)
This AC could be used to prevent injuries to the renal arteries with instruments other than the clip carrier.

This regional AC are intra-operatively defined (construction from stereo-images) while removing the fat around the kidney. This demo allows testing the design of active constraints with GUI and the AC movement and/or deformation (dynamic AC). Transformations are computed by identifying landmarks (more than 2 not aligned – leading to well conditioned equations, robust to noise) in the position in which the AC has been originally designed and the correspondent points on the displaced/deformed image/point cloud. The chosen procedure, phase and step is the most compatible with the expected unavoidable error in locating landmarks and 3D reconstruction error in the point clouds. The following picture (Figure 3) summarizes the steps bringing intraoperative AC.



D5.1: Dynamic active constraint construction

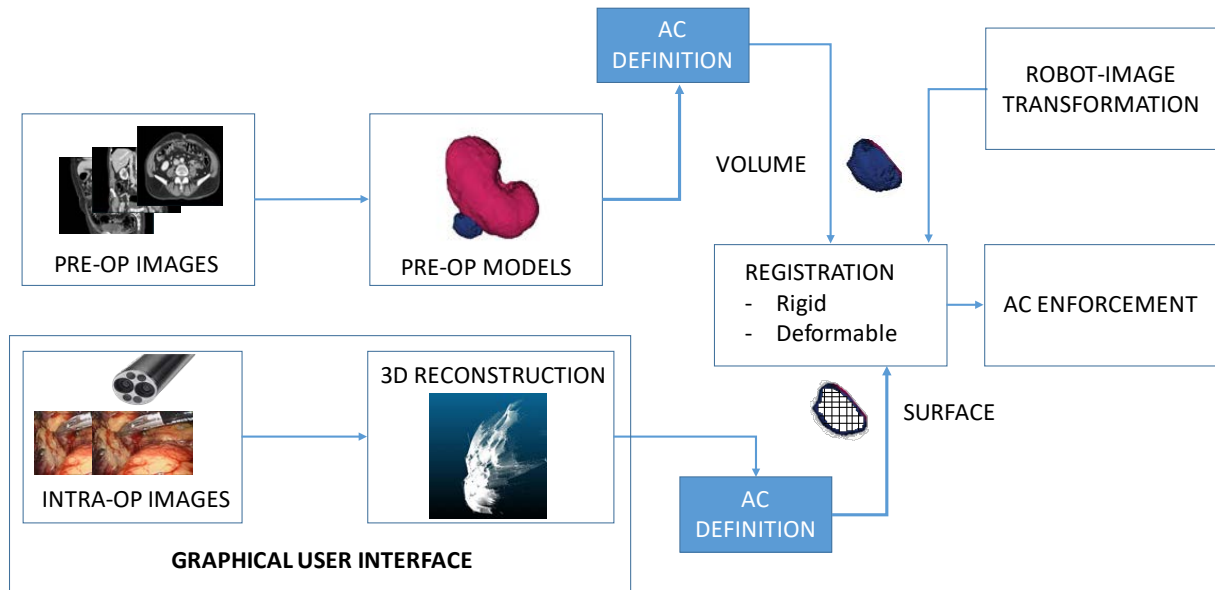


Figure 3 AC can be defined either on pre-op models or on intra-operative models. Both are registered using a rigid or deformable approach. AC provide repulsive force fields (AC enforcement – T5.2).

In order to investigate how to co-register surface or volume models segmented from the medical images (MI) on to the vision system (VS) and the robot (R) reference frame we implemented:

- **Rigid registration** methods
- **Deformable registration** methods (since displacements are due to patient ventilation and interaction with surgical tools) of exposed surfaces the point cloud (PC) of which is available.
- **Propagation of deformation** in the bulk of the organs is the most challenging research and will be implemented, in a later stage of development.

The static/dynamic AC are constructed:

- **Pre-operatively**, directly on the images dataset or on the segmented organs
- **Intra-operatively**, using the dedicated “AC definition module” and the implemented **Graphical User Interface (GUI)**

In order to test the developed tools, POLIMI developed phantom organs from models segmented on Medical Images (MI) and two testing datasets (using phantoms and butchery organs), made available to the rest of the SMARTsurg consortium



D5.1: Dynamic active constraint construction

1.2 Document Structure

This document is aimed at reporting activities of T5.1, aimed at investigating how to co-register surface or volume models segmented from the medical images (MI) on to the vision system (VS) and the robot (R) reference frame.

The document is structured by tasks as follows:

- Section 2 - Rigid and deformable registration methods
- Section 3 - Intra-operative GUI
- Section 4 - Pre-operative and intra-operative constraint regions definitions
- Section 5 - Datasets

1.3 Reference Documents

D2.1 End-users requirements, use cases and application scenarios
SMARTsurg Description of work (DOW)



D5.1: Dynamic active constraint construction

1.4 Acronyms and Abbreviations

Abbreviation	Definition
AC	Active Constraints
CT	Computer Tomography
D	Deliverable
DVRK	da Vinci Research Kit
EC	European Commission
ELAS	Efficient Large Scale Stereo Matching
EU	European Union
FFD	Non-rigid Free-From Deformation
GUI	Graphical User Interface
ICP	Iterative Closest Point algorithm
M	Month
MIS	Minimally Invasive Surgery
WP	Work package
MI	Medical Images
MRI	Magnetic Resonance Imaging
PC	Point Cloud
ROS	Robot Operating System
RaLMR	Robot-assisted Repair of Partial Lateral Meniscus Tear
RaPLM	Robot-assisted Partial Lateral Meniscectomy
RAPN	Robot-Assisted Partial Nephrectomy
RARC	Robot-Assisted cystectomy and intracorporeal Reconstruction
RARP	Robot-Assisted Radical Prostatectomy
SGM	Semi-Global Matching
VS	Vision system
VF	Vector Field



2 Registration

The registration step aims at aligning the organ anatomy, retrieved from pre-operative computed-tomography (CT) images, with the intra-operative view, acquired with endoscopic cameras.

In particular, the vertices (M) of the pre-operative organ model can be registered onto the reconstructed intra-operative moving point-cloud (F), which is obtained after 3D reconstruction of the model (T3.1). However, this will be in conjunction with the 3D registration performed in T3.3.

We implemented three registration approaches, i.e. pair-point registration, surface-based rigid registration and surface-based deformable registration, which we will discuss in the next sections.

2.1 Pair-point registration (Rigid Landmark-based registration)

In the pair-point registration approach, the registration was performed between two sets of corresponding points, called landmarks: the first set (L_M) was a subset of M , while the second one (L_F) was a subset of F . L_M and L_F were selected as to be clearly visible on both M and F (Figure 4).

The spatial (rigid) transformation T between L_M and L_F was obtained by minimizing the Euclidean distance between sets L_F and $T(L_M)$.

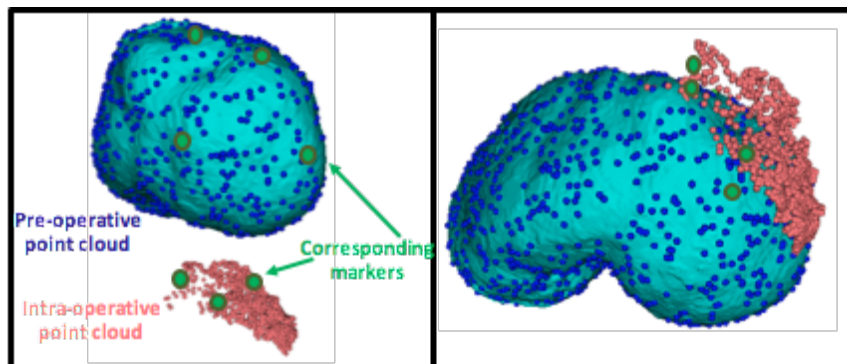


Figure 4 Pair-point registration of the kidney model to the intra-operative kidney point cloud. (Left) The pre-operative point cloud (M) is shown in blue and the simulated intra-operative point cloud (F) in pink. Anatomical landmarks, manually selected through a graphic-user interface, are shown in green both for M (L_M) and for F (L_F). (Right) The computed pair-point registration is applied to register the pre-operative point cloud into the intra-operative scene.

2.2 Surface-based rigid registration

Once we achieve the pair-point registration, the registration between M and F was refined with a surface-based rigid registration algorithm. The surface-based rigid registration was described by a transformation with six degrees of freedom in 3D, three for rotation and three for translation. The underlying hypothesis is the rigidity of the structures. For surface-based rigid registration, we implemented the Iterative Closest Point (ICP) (Besl et al., 1992; Zhang, 1994), as it has low computational complexity. The initialization is important for this algorithm, possibly



D5.1: Dynamic active constraint construction

leading to local minima. The marker based has shown to be reliable enough for the convergence to a global minimum.

2.3 Deformable surface registration

Rigid registration did not allow tacking into account tissue deformation. Thus, we investigated the use of surface-based deformable registration. The associated transformation can be described by from six up to infinite degrees of freedom, since the deformation model can be selected as complex as desired.

Vector Field (VF) is among the most successful surface-based registration approaches. VF can be seen as a grid in which each block has associated a displacement vector, in terms of direction and intensity, as shown in Figure 5. The grid is superimposed on the moving point cloud M . The deformation is represented as the deformation of an underlying mesh of $n_x \times n_y \times n_z$ control points $\phi_{i,j,k}$ with uniform spacing of the mesh Φ . Each control point displacement is found minimizing a cost function based on the Euclidean distance of the two point sets.

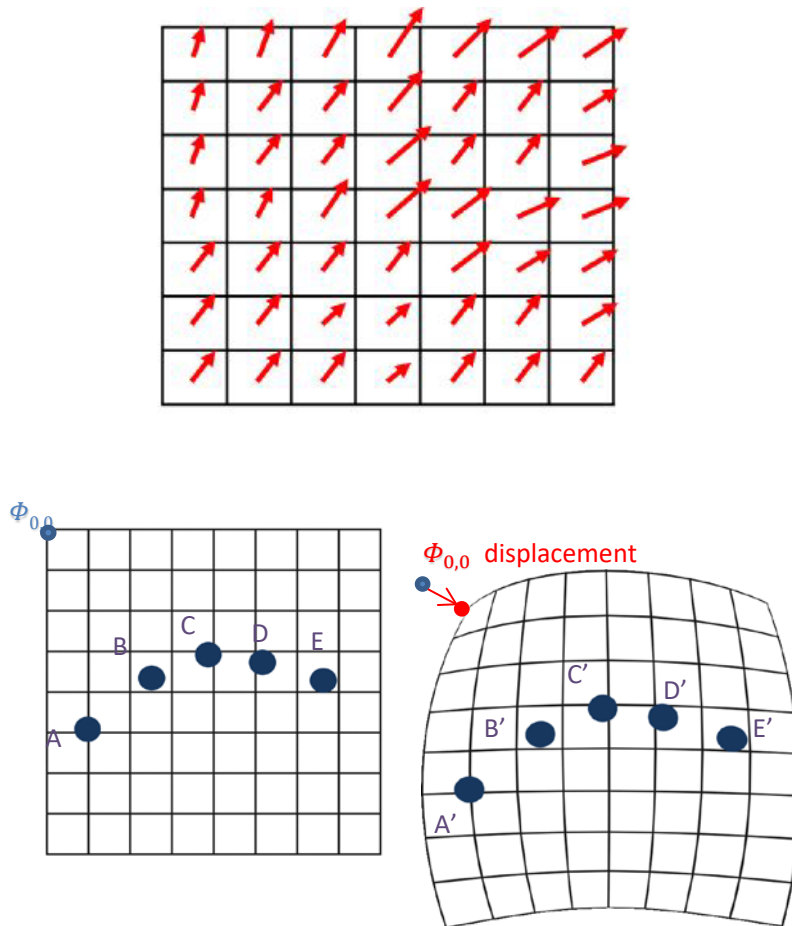


Figure 5 The VF (upper panel) describes surface-based deformable registration. VF can be seen as a grid superimposed to the pre-operative point set, in which each block has associated a displacement vector, representing the direction and the size of the translation applied to what is inside that block. In the lower panels, the deformed (right) and initial (left) position of exemplary points is reported.



D5.1: Dynamic active constraint construction

To compute the displacement vectors, we decided to exploit the non-rigid Free-From Deformation (FFD) based on B-spline (Rueckert et al., 1999, Sederberg et al., 1996) (Figure 6).

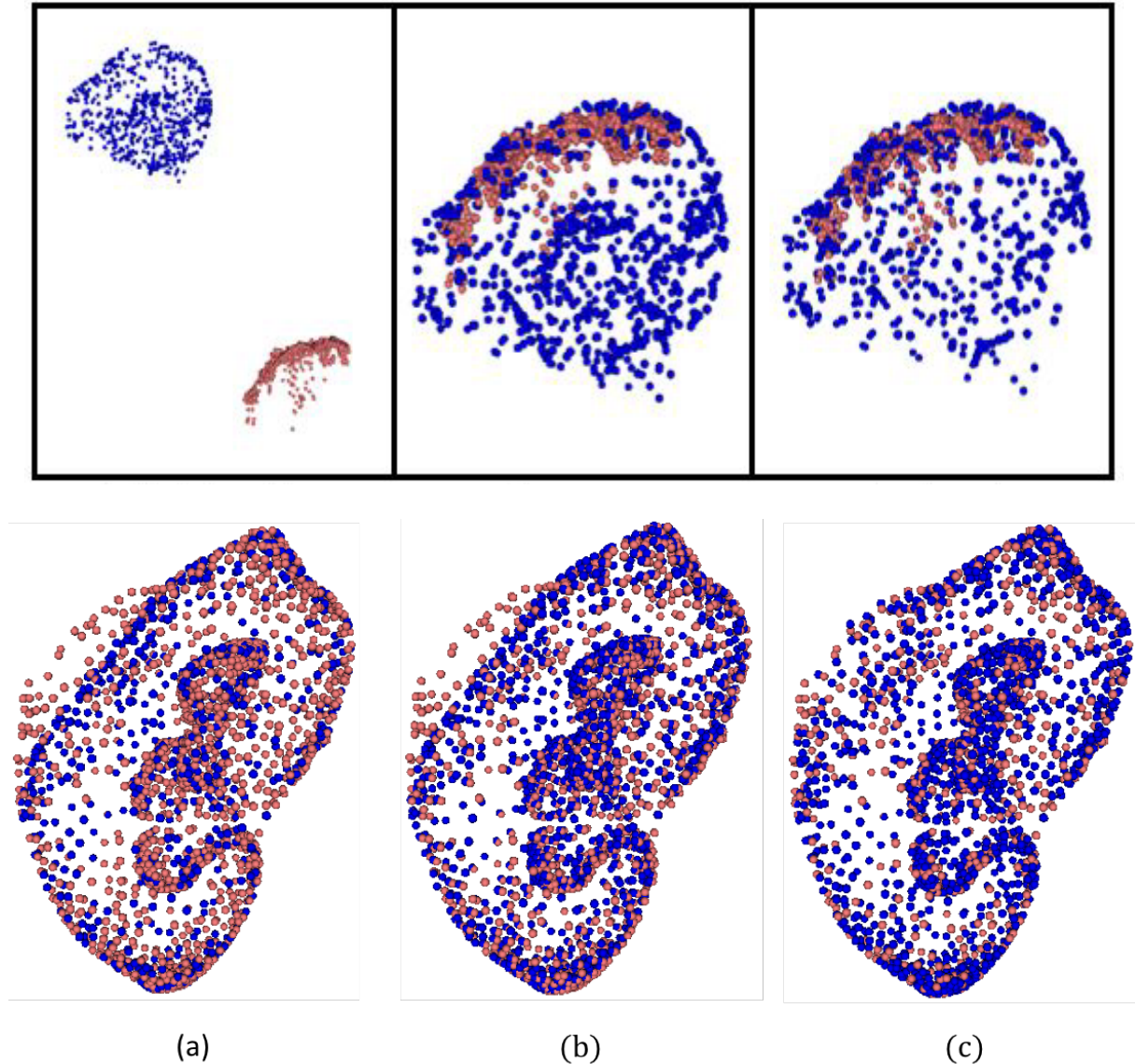


Figure 6 FFD results. (Upper panel on the left) Initial situation: the blue point cloud refers to the pre-operative model and the pink point cloud to the intra-operative phantom-kidney surfaces. (Upper panel in the middle) Rigid registration with ICP, the initial alignment was performed with the pair-point registration. (Upper panel on the right) Registration refinement was performed with surface-based deformable registration. On the lower panel, a slice is represented for better visualization: (a) Pre-operative model vertexes (blue) and intra-operative point cloud (red). The registration is obtained with (b) iterative closest points (ICP) and (c) free-form deformation based on B-splines

Accuracy evaluation has been carried out between FFD and ICP. The following graph (Figure 7) reports RMSE percentage variation of FFD and ICP results (RMSE final) with respect to the first rigid transformation (RMSE initial) with pair-point matching.



D5.1: Dynamic active constraint construction

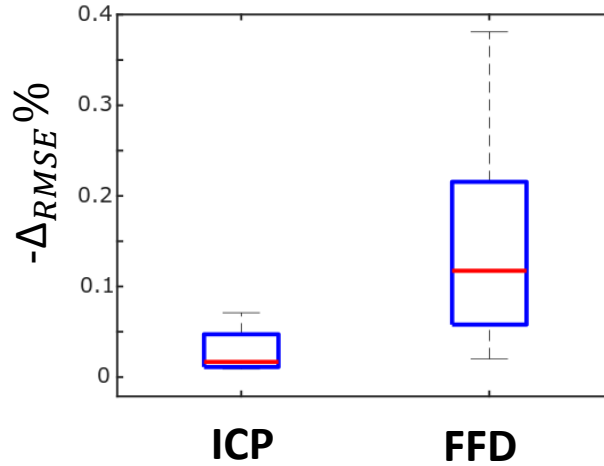


Figure 7 RMSE percentage variation after applying ICP and FFD algorithms. A better performance of FFD is evident from the Box plots.

$$-\Delta_{RMSE} \% = \frac{RMSE_{initial} - RMSE_{final}}{RMSE_{initial}} * 100$$

Difference is significant with $\alpha=0.05$ in the Wilcoxon test.

Residual errors in AC positioning are due to:

- Errors on the point cloud (noisy or too smooth)
- Errors in the manual selection for pair-points matching
- Errors in the registration (rigid or deformable)
- Errors in the propagation of the superficial deformation to internal structures and to AC (actually non present in pure surface AC)
- Errors due to the computational time required by the registration process

All the modules for registration are available at the following GitHub link:

https://gitlab.com/Polimi-dVRK/dvrk/dvrk_registration_module.



D5.1: Dynamic active constraint construction

3 Intra-operative Graphical User Interface (GUI)

The intraoperative GUI is based on Unity. Since the programming language used by Unity is C#, wrappers to C++ were implemented to communicate via ROS with the other components of the surgical robot (i.e. master arms, slave arms, endoscope) and of the vital-signals measurement devices (e.g. ECG). Figure 8 represents how the different parts of the system communicates between each other.

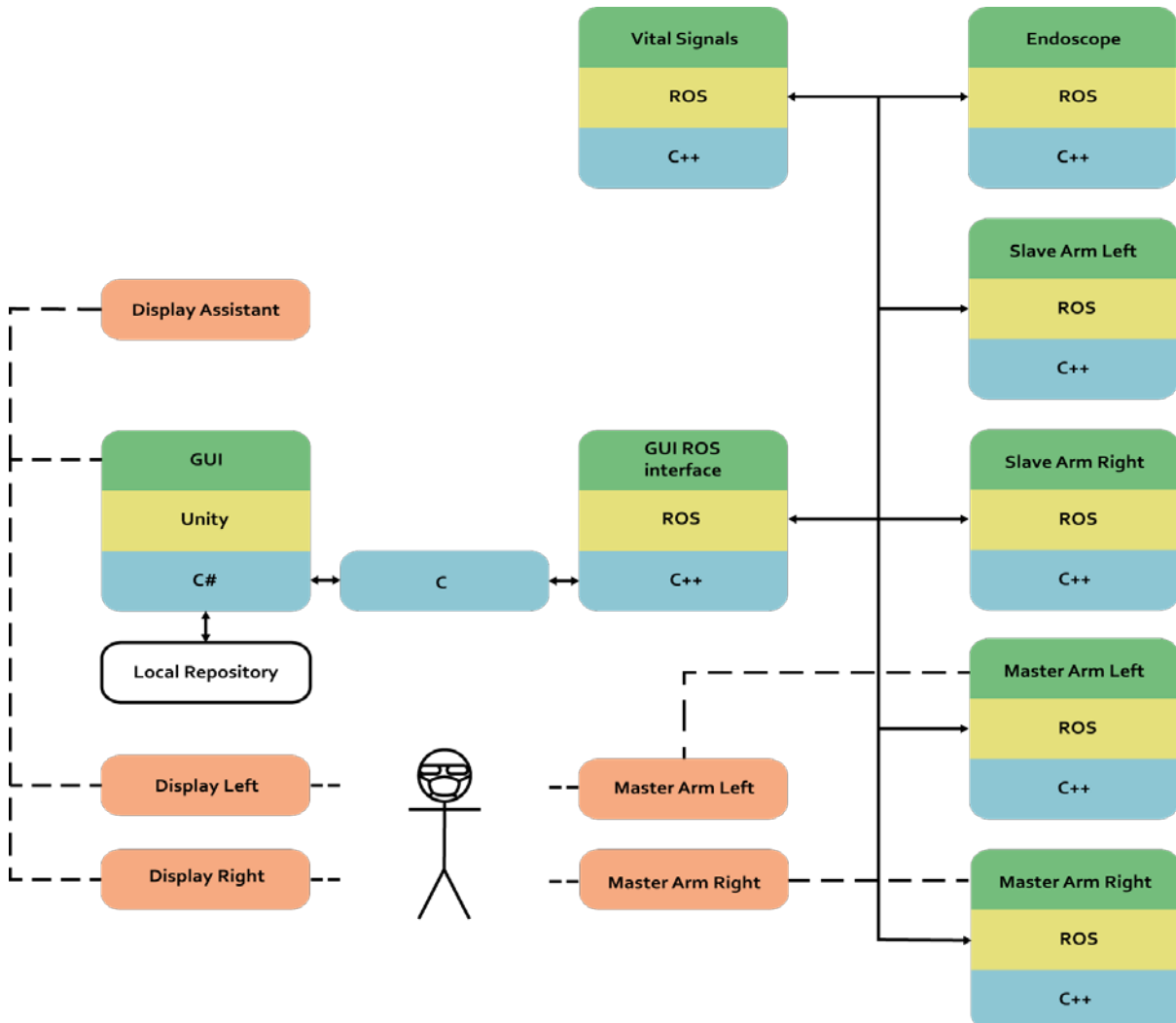


Figure 8 Block scheme of the GUI. Orange blocks represent the hardware components, green blocks represent high-level components, yellow blocks represent middleware and blue blocks represent the programming languages used for the implementation. Solid arrows are used to show how blocks communicates each other, while dashed lines to show how a human interact with the system.

The developed code uses the following libraries:

- Unity 2018.1.0b8
- ROS kinetic
- [Opencv 3.0](#)
- The dVRK (da Vinci Research Kit) software



D5.1: Dynamic active constraint construction

3.1 GUI Main window



Figure 8 GUI and main windows on the figure corners.

The main window of the intraoperative GUI allows the surgeon to see the images from the endoscope during the whole procedure. To obtain the depth perception, the images from the stereo-endoscope are displayed on two different screens. An optional third monitor can be used to display either the left or the right endoscopic image. Four buttons placed at the corners of the screen are overlaid on the endoscope images and are used to access the different GUI windows (Figure 8). The meaning of the four buttons is explained in Table 2





	Open/close preoperative models window
	Open/close AC (active constraint) window
	Open/close vital signs window
	Open/close camera window

Table 2 Symbols used in the intra-operative GUI



D5.1: Dynamic active constraint construction

3.2 Preoperative Models Window

Preoperative digital models of organs (in *.obj* format) are uploaded asynchronously during the awakening procedure of Unity from the storage memory of the device hosting the GUI. The display of the preoperative models is controlled by the buttons/sliders of the 'Preoperative Models window' (see figure 9) opened using the top-left-corner button. The slider appearing in the window is used to control the transparency of the organ models, whereas the three triangular buttons on its left are used to set the visualization modality as follows from top to bottom: mesh, wireframe or point-cloud.

Figure 9 shows how the models of a kidney (cyan) and of a liver (magenta) are rendered in the preoperative-models window (top left corner of the GUI). Within this environment, models can be magnified, rotated and translated (to be implemented).

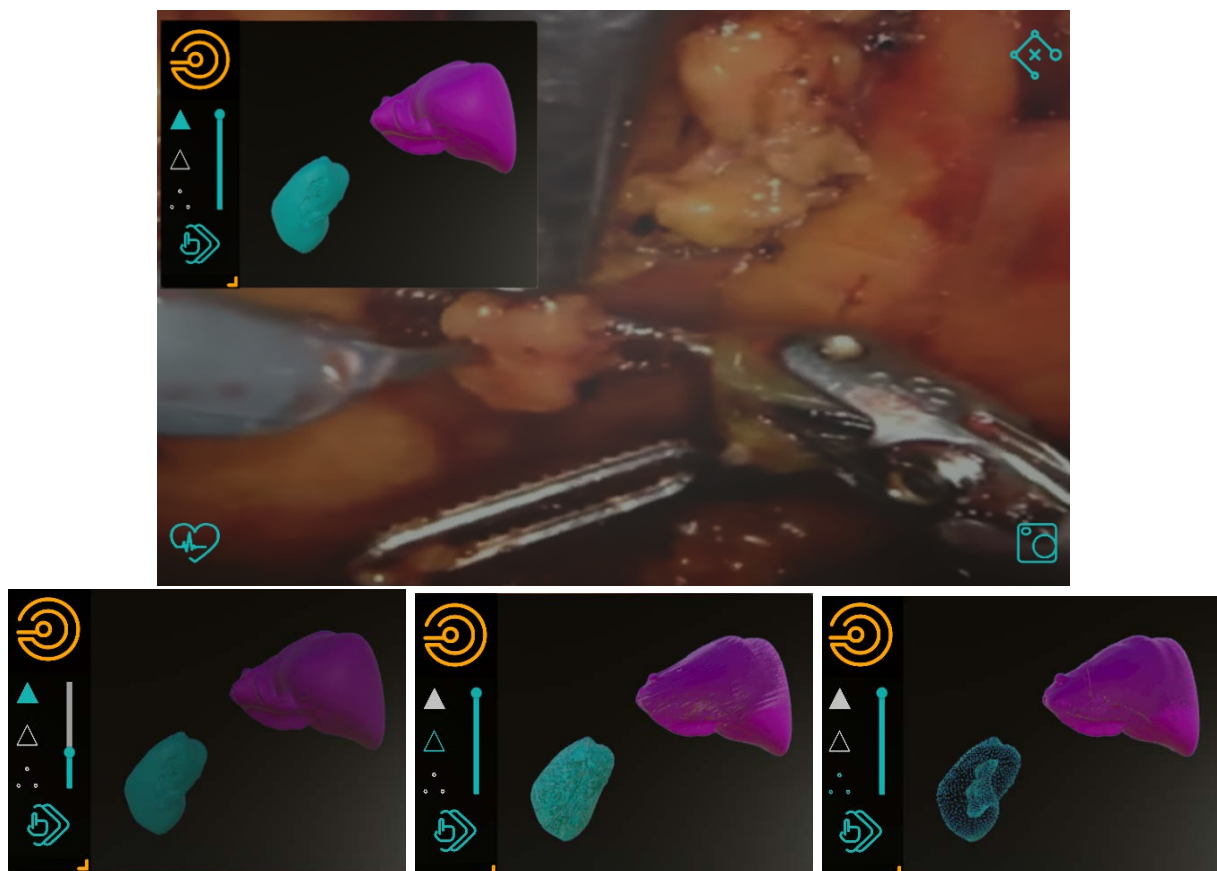


Figure 9 Full-preoperative-models window (with VR environment rendering) for models manipulation and exploration. The top image shows the positioning of the window during the surgery. The bottom line represent three different modalities of visualization: mesh with low transparency, wireframe and point-cloud.

3.3 AC window

From this window (upper right corner in Figure 10) AC can be drawn moving a cursor on a planar surface placed above the point cloud of the intraoperative surgical scene (see Section 4.2). The drawn AC can be visualized and hidden using the "Visual AC" toggle. The "Actual AC" toggle is used to switch on/off force rendering of the active constraints.



D5.1: Dynamic active constraint construction

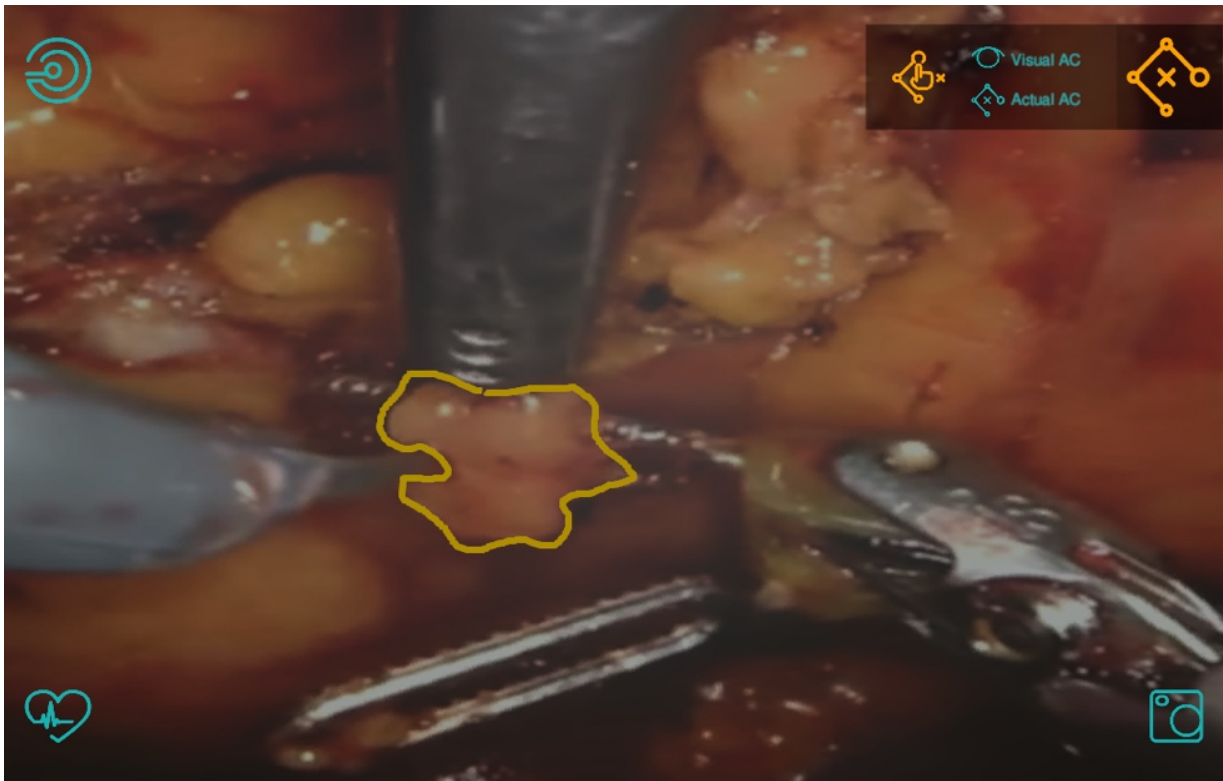


Figure 10. On the upper right corner the AC windows is shown. AC can be visualized and hidden using the “Visual AC” toggle. The “Actual AC” toggle is used to switch on/off force rendering of the active constraints. A yellow line is reported, which delimits a safety area on a plane placed between observer and 3D scene (see also Figure 17 in 4.2)

3.4 Vital Signals Window

This window is used to display the vital signs specified by the surgeons. The surgeon will set the preferred signals during an initialization procedure where he/she will log in his/her personal profile. Vital signs are received from ROS and, up to now, three type of messages are accepted: *std_msgs::Float64*, *std_msgs::String* and *std_msgs::bool*. To simulate the signal represented in Figure 10, a ros node publishes a real ECG signal stored on a computer connected to the robot-network.

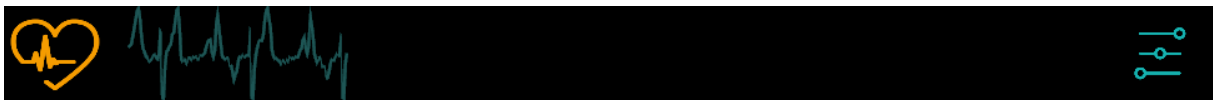


Figure 11 vital signs window with ECG signal

3.5 Camera Window

The functions of this window have to be still implemented; in it's current form, it is a first graphical draft that might be still changed after further consultations with clinical partners. The basic idea is that by controls present in this window, the surgeon will be able to record a video of the surgery, to take pictures, to move the camera using the GUI and to zoom the operating scene with a digital zoom.



3.6 Repository with code

All the developed code, the installation instructions and the updated status of the GUI can be found on the [Polimi-dVRK GitLab](#). The *SMARTsurg_GUI* folder contains the code developed in C# and the Unity files of the GUI. The *ros_interface_plugin* directory contains all the C and C++ to manage the communication of the GUI with ROS. *Preoperative models* contains preoperative models for testing purposes.



D5.1: Dynamic active constraint construction

4 AC definition

4.1 Pre-operative AC definition

A module to segment abdominal organs and tumors has been developed in 3D Slicer (<https://www.slicer.org/>).

The module is made of the following sections:

- A. *Load DICOM images*
- B. *Modify images*
- C. *Set seeds*
- D. *Start segmentation*
- E. *Generate models*

The module allows loading preoperative DICOM CT/MR volumes (A). The DICOM volumes can be modified (B), e.g. to adjust the image contrast and better enhance structures of interest. As a prerequisite for the segmentation, the user is asked to manually insert seed points (C) on structures of interest (i.e., organs to be segmented). An active contour segmentation algorithm (Gao et al., 2012) is exploited to automatically obtain the organ segmentation mask from the seed points (D). Once the organ segmentation is obtained, the 3D surface models from segmented data is generated (Lorensen et al., 1987) (E), as shown in Figure 12-13 and 14.

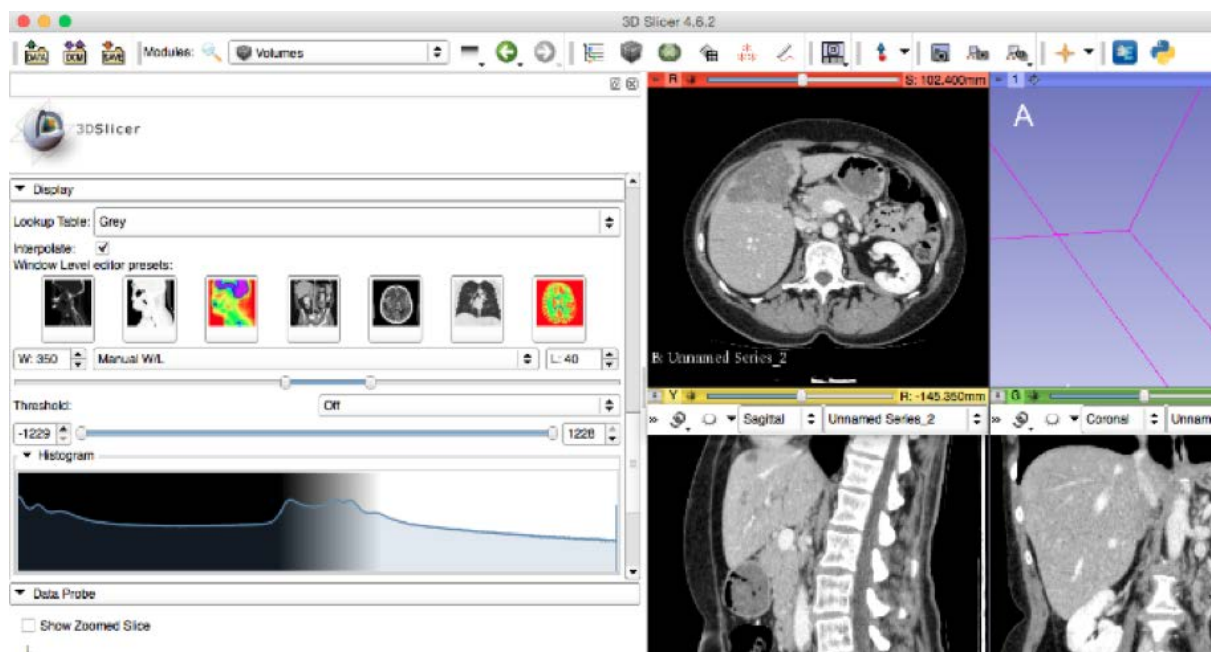


Figure 12 GUI for model segmentation (3D Slicer)



D5.1: Dynamic active constraint construction

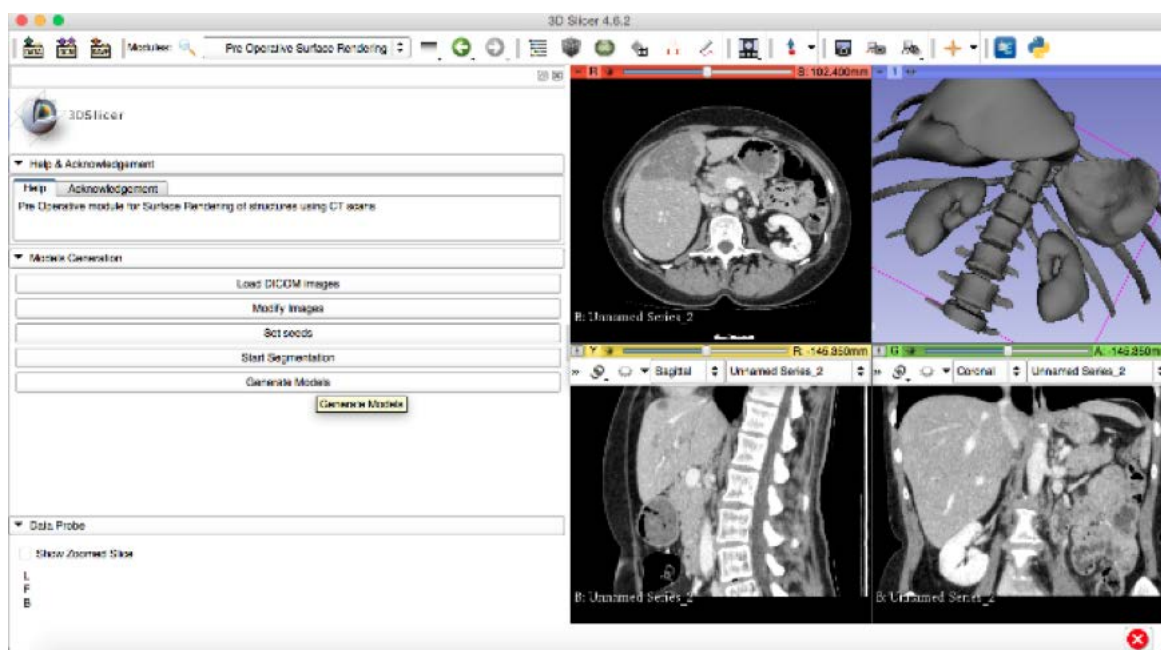


Figure 13 Generated 3D model from the segmented organs (bone, liver, spleen, kidneys).

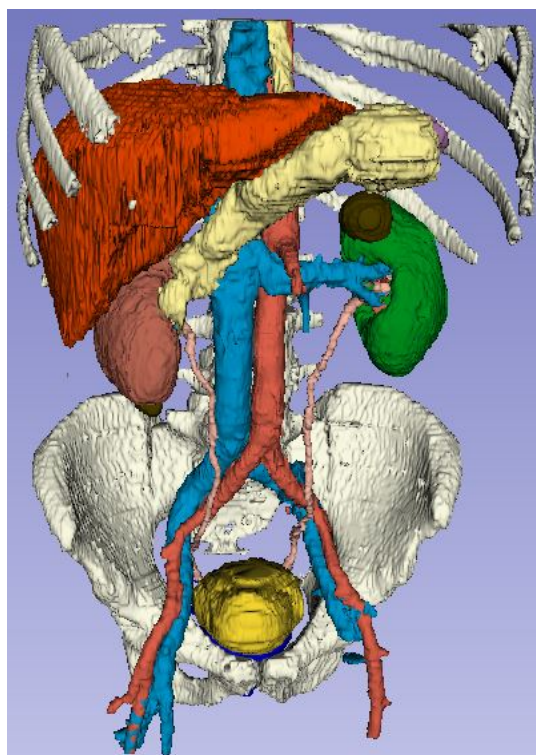


Figure 14 Pre-operative organ models for constraint definition. Straw yellow: stomach; orange: liver; green: left kidney (with the cancer highlighted in brown); blue: inferior vena cava and renal veins; red: aorta; pink: ureters; intense yellow: bladder; white: chest and pelvis bones.



D5.1: Dynamic active constraint construction

4.2 Intra-operative AC definition

A general method (independent from preoperative images and initial alignment) for generating intraoperative AC around physical objects within a robot's workspace, entails the step of brushing the surface of the body portion that must not be damaged accidentally (e.g. vessels, nerves,...). A virtual surface is needed to support that brushing. It is not possible indeed to paint on an image coming from cameras of an endoscope (as a general example of stereo viewer) since no numerical data are available on the depth, albeit the latter is well perceived by the operator with stereo vision through innate brain elaboration.

Such a virtual supporting surface is represented by the 'scene' in virtual simulators, or can be obtained by the stereo disparities detected on the stereo pairs.

The basic principle involved in the recovery of depth using passive imaging is triangulation. Hence a correspondence needs to be established between features from two images that correspond to some physical feature in space. The most used algorithms to find correspondences between two images are:

- **SIFT** (Scale Invariant Feature Transform) extracts distinctive invariant (to image scale and rotation) features from images. It consists of four major stages: scale-space extrema detection, keypoint localization, orientation assignment and keypoint descriptor (Juan et al., 2009).
- **SURF** (Speeded-Up Robust Features) relies on integral images for image convolutions; by building on the strengths of the leading existing detectors and descriptors. Due to the use of integral images, it filters the stack using a box filter approximation of second-order Gaussian partial derivatives (Bay et. al. 2008)
- **ELAS** (efficient large scale stereo matching) is an approach to binocular stereo for fast matching of high resolution imagery. It builds a prior on the disparities by forming a triangulation on a set of support points which can be robustly matched, reducing matching ambiguities of the remaining points. This allows for efficient exploitation of the disparity search space, yielding accurate and dense reconstructions without global optimization. Also, the method automatically determines the required disparity search range (Geiger et al. 2011).
- The **quasi dense stereo matching** algorithm proposed by Stoyanov et al. It first recovers a sparse set of matches across the image pair using a feature based technique. With a sparse set of 3D points it then propagates 3D information to cover a semi-dense portion of the scene. During the first stage all features correspondences are used as seed matches. They are sorted subject to the correlation score between their respective templates and stored using a priority queue structure. The algorithm then proceeds to propagate structure around the matches with highest correlation scores on a best-first basis by popping the priority queue. New matches are simply added to the queue as the algorithm iterates until no more matches can be popped. (Stoyanov et al. 2010)



D5.1: Dynamic active constraint construction

In any case, three-dimensional (3-D) reconstruction of surfaces (triangulated meshes) is an issue related to processing time, so that the use of unstructured raw data (i.e. point clouds) is currently more widespread within the literature (Hoppe et al. 1992, Li et al. 2005).

There are various methods for computationally representing active constraints. Simple methods using points, lines, and planes, while more complex methods exploit polygonal meshes and parametric surfaces. Polygonal meshes provide great flexibility for representing constraint geometries (Figure15), but they are considerably more complex to construct, evaluate, and store than the simpler representations.

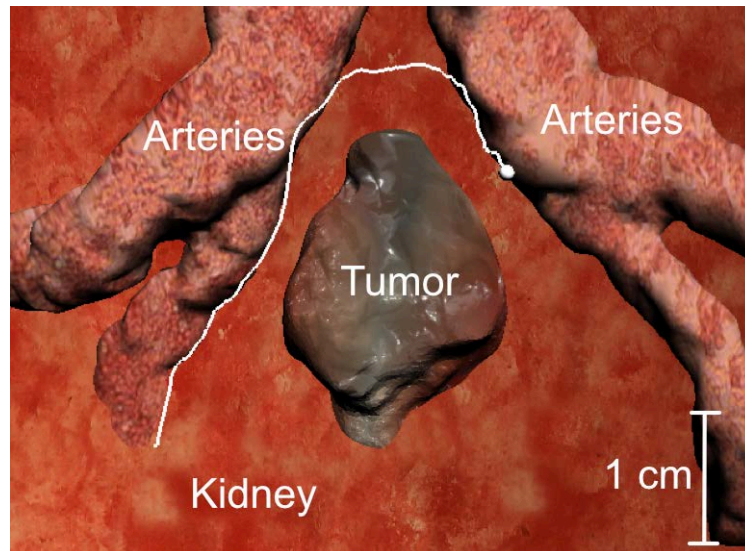


Figure 15. AC design in virtual world where the surfaces are represented with polygonal meshes. The pointer for actual surface brushing is indicated with a small white sphere. Picture refers to a kidney surface (reddish background) on which an esophytic tumour is located and the renal arteries enter the parenchyma.



D5.1: Dynamic active constraint construction

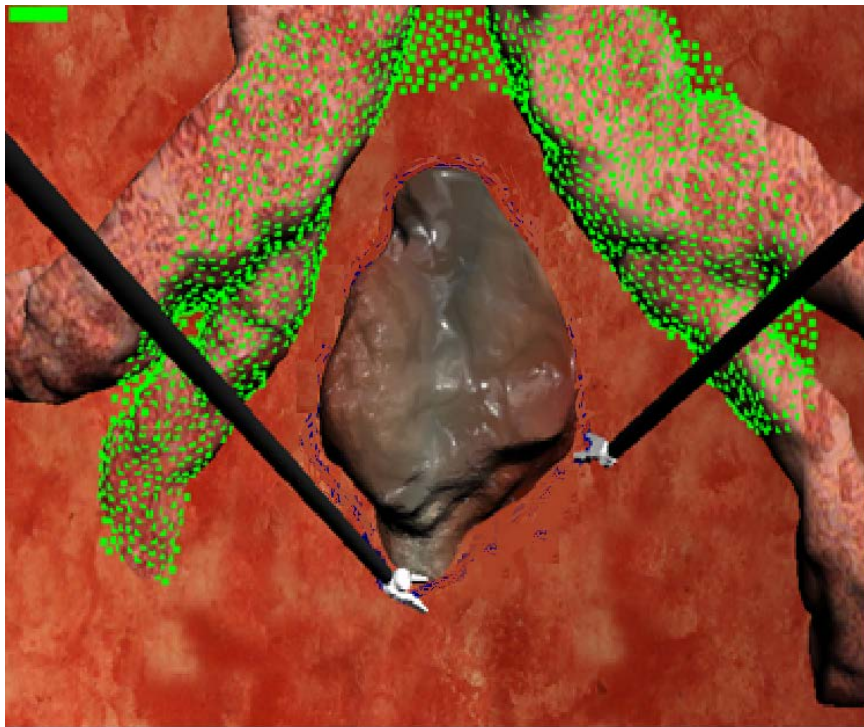


Figure 16 AC point cloud (light green spots) has been designed on the virtual surface on the renal arteries.

The developed GUI, as described in Section 3.3, is used for the definition of the point clouds, which model the AC. The used technique (Figure 17) deploys a virtual plane (reported in Figure 17 as safety area plane) placed between the observer (viewpoint) and the point cloud (3D scene). On this plane, using a mouse or a master robotic-arm, the surgeon can draw an area to delimit the AC (indeed its projection, see Figure 10 in section 3.3, yellow line and safety area plane in Figure 17).



D5.1: Dynamic active constraint construction

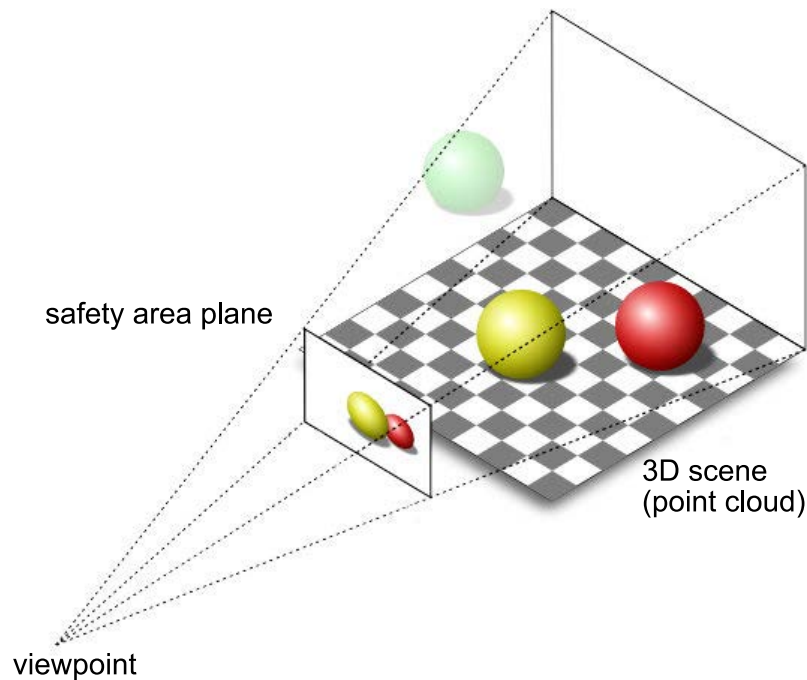


Figure 17. Structure of the projection of 3D scene on the plane where safety areas are drawn.

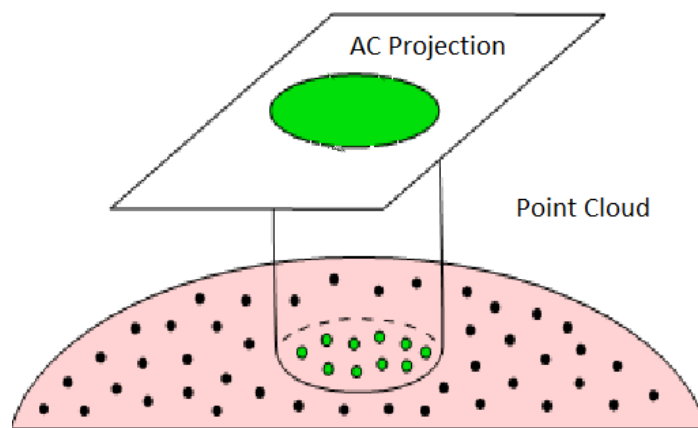


Figure 18. Projecting Point cloud on a 2D plane where the AC contour is then drawn (polygon bounding the green area) and projecting the points inscribed in green area back to the 3D scene, identifies the points belonging to the AC as a point cloud (green spots).

The projection of the points included in the safety area projected on the plane back to the 3D scene identifies the points belonging to the AC as a point cloud (i.e. defines the AC to be rendered visually and haptically).

This step is of fundamental importance since the selected points will be used to reconstruct the 3D surface of the anatomical structure that will form the AC volume, from which the surgical tool will be steered away. The problem is defined in the 3D space, so the primary challenge consists in identifying the 3D points confined within a 2D polygon seen from the perspective point of the user who drew the area.



D5.1: Dynamic active constraint construction

To solve the problem it was decided to transform the 3D formulation into a 2D one. Instead of projecting the AC on a parallel plane beyond the scene to create a polyhedron, it turned out to be more convenient to project the point cloud on the same plane of the AC (Figure 17). Following this step, by applying a 2D ray-casting algorithm, it is possible to identify the points inside the polygon and then project them back to their original position to obtain the points of the safety volume's surface.

The last problem to be solved is to identify points lying within (internal) and outside (external) of the closed line identifying the AC on the safety area plane. This identification has been done by the classic point-in-polygon (PIP) problem based on the Jordan Curve Theorem. This method identifies the included points by running semi-infinite rays out from the points, and counting how many edges they cross (Figure 19).

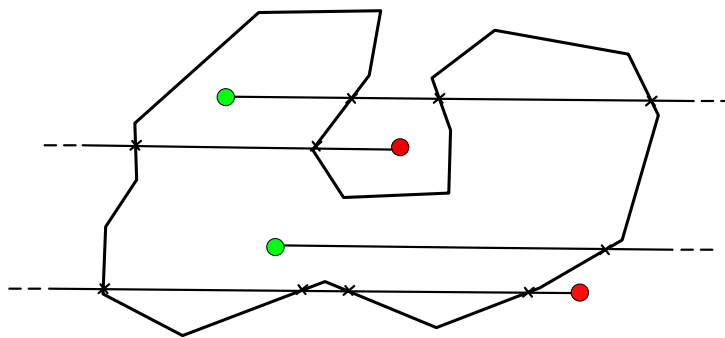


Figure 19. Point in polygon problem

The point p belongs to A (inner surface) if the ray through p in a fixed direction intersects P (Poly line surrounding AC) in an even number, 0, 2, 4, 6, ..., of points.

The point p belongs to B (outer surface) if the ray through p in the fixed direction intersects P in an odd number, 1, 3, 5, ..., of points.

The following Figure summarizes the procedure.



D5.1: Dynamic active constraint construction

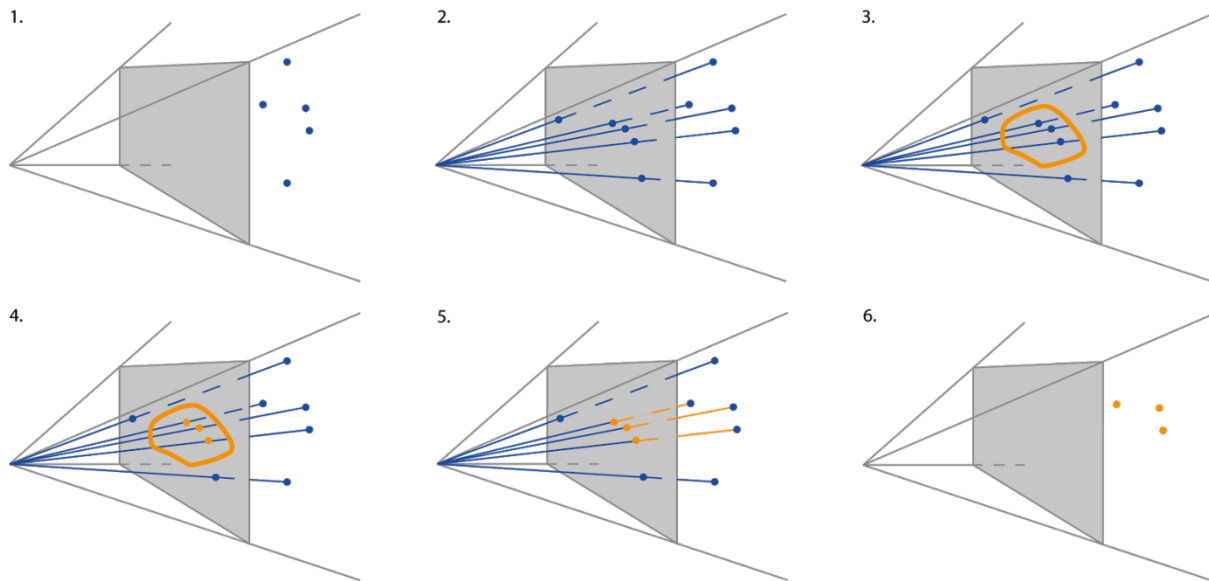


Figure 20: (1) a virtual plane is defined between the observer (intersection of the grey lines) and the object (blue 3D-points); (2) 3D-points are projected on the virtual plane; (3) an area is drawn on the plane to define the AC; (4) points within the area are identified and (5) associated to their corresponding 3D-point to define the 3D-AC (6)



D5.1: Dynamic active constraint construction

5 Datasets

At POLIMI two datasets were prepared, using plastic phantoms and butchery organs. The dataset contains RGB, infrared and depth images of biological tissues (veal kidney, liver and fat) using a daVinci surgical system endoscope (576x720px frame, 30Hz, Intuitive surgical, USA) and an Intel Realsense D435 camera (Intel corporation, USA).

The dataset complete and exhaustive description is available at the following link:
https://gitlab.com/Polimi-dVRK/dvrk/dvrk_ex_vivo_dataset_tools/tree/master

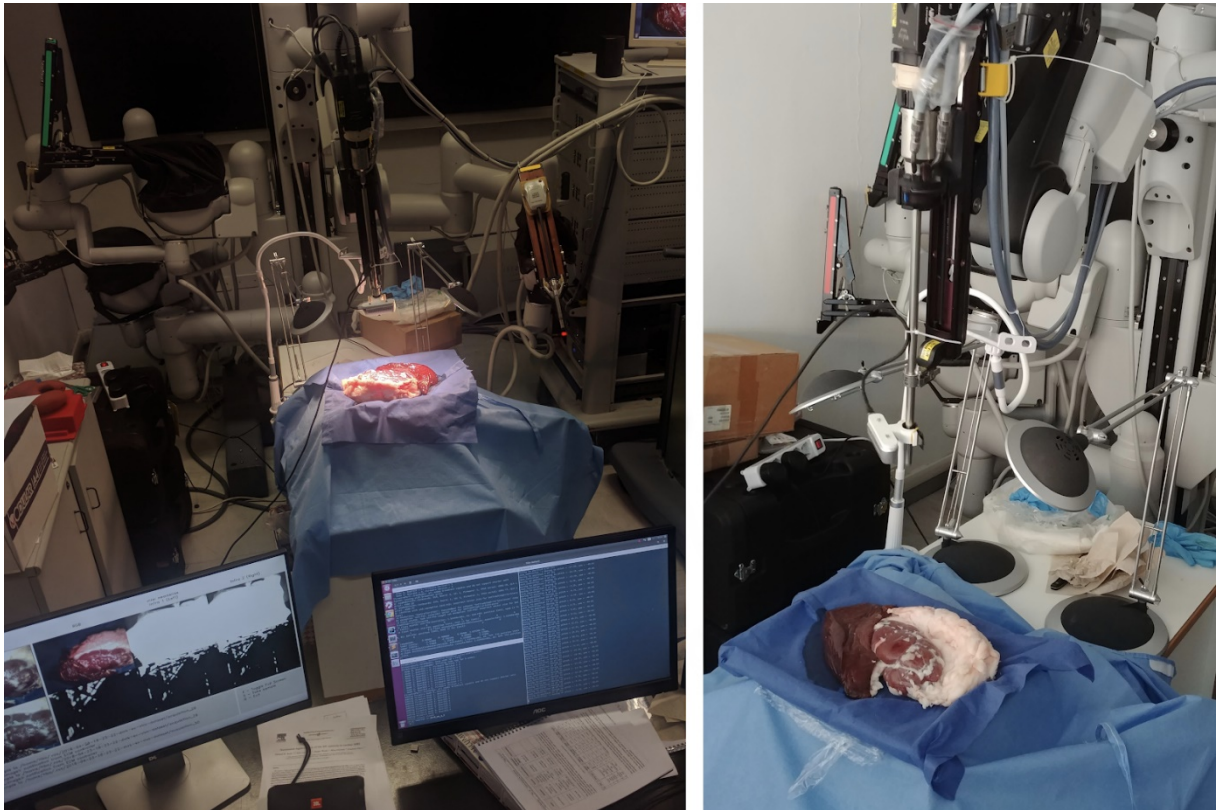


Figure 21 Experimental setup for dataset acquisitions at POLIMI.

The use of the dataset is to made available to relevant partners a way to test convergence of algorithms for 3-D textured point cloud extraction from stereo images. The use of butcher material instead of the silicon phantoms is due to the fact that these latter lack of the needed texture for on-the-fly 3-D surfaces computation.



D5.1: Dynamic active constraint construction

6 Conclusion

D5.1 in its current release describes the processes for the definitions of constrained regions to be preserved during the selected demonstration scenarios. We have implemented methods for:

- Building pre-operative models starting from pre-operative images
- Registering pre-operative models into the intra-operative scenario
- Building intra-operative models from 3D reconstructed surfaces.

In D5.1 we provide links to Software modules and interfaces, as well as link to a dataset for 3D reconstruction testing.

- Further developments (due at month 26) will be related to:
- Completion of the integration of Unity GUI in a ROS environment in order to build a stand-alone application
- Methods for surface deformation propagation within the internal structure of the organ to track deep targets during possible deformations due to interaction with surgical tools using graphic libraries with dynamic properties, energy propagation approaches and machine learning for real-time estimation.



D5.1: Dynamic active constraint construction

7 References

Bay, H., Ess, A., Tuytelaars, T. & Van Gool, L., 2008, Speeded-up robust features (SURF). Computer vision and image understanding, 110(3), 346-359.

Besl, P.J., McKay, N.D, et al., 1992, A method for registration of 3D shapes, IEEE Transactions on pattern analysis and machine intelligence, vol. 14, no. 2, pp. 239-256.

Bowyer, S.A., Davies, B.L. & Rodriguez y Baena F., 2014, Active Constraints/Virtual Fixtures: A Survey. IEEE Transactions on Robotics: A Publication of the IEEE Robotics and Automation Society, 30(1), 138–157.

Chen, Z., Malpani, A., Chalasani, P., Deguet, A., Swaroop Vedula, S., Kazanzides, P. & Taylor, R. H., 2016, Virtual fixture assistance for needle passing and knot tying. In 2016 IEEE/RSJ International Conference on Intelligent Robots and Systems (IROS). <https://doi.org/10.1109/iros.2016.7759365>

Enayati, N., Alves Costa, E.C., Ferrigno, G., & De Momi, E., 2016, A dynamic non-energy-storing guidance constraint with motion redirection for robot-assisted surgery. In 2016 IEEE/RSJ International Conference on Intelligent Robots and Systems (IROS). <https://doi.org/10.1109/iros.2016.7759634>

Gao, Y., Kikinis, R., Bouix, S., Shenton, M. & Tannenbaum, A., 2012, A 3D Interactive Multi-object Segmentation Tool using Local Robust Statistics Driven Active Contours, Medical Image Analysis, <http://dx.doi.org/10.1016/j.media.2012.06.002>

Geiger, A., Ziegler, J., & Stiller, C., 2011, Stereoscan: Dense 3d reconstruction in real-time. In Intelligent Vehicles Symposium (IV), 2011 IEEE (pp. 963-968). Ieee.

Juan, L., & Gwun, O., 2009, A comparison of sift, pca-sift and surf. International Journal of Image Processing (IJIP), 3(4), 143-152.

Lorensen, W.E. & Cline, H.E., 1987, Marching cubes: A high resolution 3D surface construction algorithm." SIGGRAPH '87 Proceedings of the 14th annual conference on Computer graphics and interactive techniques. Pages 163-169. ACM New York, NY, USA.

Rosenberg, L.B., 1993, The use of virtual fixtures to enhance operator performance in time delayed teleoperation. PsycEXTRA Dataset. <https://doi.org/10.1037/e477812004-001>

Rosenberg, L.B., 1993, Virtual fixtures: Perceptual tools for telerobotic manipulation. In Proceedings of IEEE Virtual Reality Annual International Symposium. <https://doi.org/10.1109/vrais.1993.380795>

Rueckert D., Sonoda L.I., Hayes, C., Hill, D.L., Leach, M.O. & Hawkes, D.J., 1999, A non- rigid registration using free-form deformations: application to breast mr images," IEEE Transactions on Medical Imaging, vol. 18, no. 8, pp. 712-721.

Sederberg, T.W. & Parry, S.R., 1986, A free-form deformation of solid geometric models," ACM SIGGRAPH computer graphics, vol. 20, no. 4, pp. 151-160.

Stoyanov, D., Scarzanella, M.V., Pratt, P., & Yang, G.Z., 2010, Real-time stereo reconstruction in robotically assisted minimally invasive surgery. In International Conference on Medical Image Computing and Computer-Assisted Intervention (pp. 275-282). Springer, Berlin, Heidelberg.

Zhang, Z., 1994, Iterative point matching for registration of free-form curves and surfaces," International journal of computer vision, vol. 13, no. 2, pp. 119-152.

Hoppe, H., DeRose, T., Duchamp, T., McDonald, J. & Stuetzle, W., 1992, Surface reconstruction from unorganized points, Comput. Graph., vol. 26, no. 2, pp. 71–78.



Reference	:	SMARTsurg-WP1-D1.1-v0.1-UWE
Version	:	1.0
Date	:	2018.06.01
Page	:	36

D5.1: Dynamic active constraint construction

Li, M., Kapoor, M. & Taylor, R.H., 2005, A constrained optimization approach to virtual fixtures. In: International Conference on Intelligent Robots and Systems pp. 1408–1413.